

# Data-Driven Event Identification Using Deep Graph Neural Network and PMU Data

Yuxuan Yuan, *Graduate Student Member, IEEE*, Zhaoyu Wang, *Member, IEEE*, and Yanchao Wang

**Abstract**—Phasor measurement units (PMUs) are being widely installed on power transmission systems, which provides a unique opportunity to enhance wide-area situational awareness. One essential application is to utilize PMU data for real-time event identification. However, taking full advantage of all PMU data in event identification is still an open problem. Hence, we propose a novel event identification method using multiple PMU measurements and deep graph neural network techniques. Unlike the previous models that rely on data from single PMU and ignore the interactive relationships between different PMUs or use multiple PMUs but determine the functional connectivity manually, our method performs interactive relationship inference in a data-driven manner. To ensure the optimality of the interactive inference procedure, the proposed method learns the interactive graph jointly with the event identification model. Moreover, instead of generating a single statistical graph to represent pair-wise relationships among PMUs during different events, our approach produces different event identification-specific graphs for different power system events, which handles the uncertainty of event location. To test the proposed data-driven approach, a large real-world dataset from tens of PMU sources and the corresponding event logs have been utilized in this work. The numerical results validate that our method has higher identification accuracy compared to the existing methods.

**Index Terms**—Event identification, interaction graph inference, phasor measurement units, deep graph neural network.

## I. INTRODUCTION

Power systems are in need of better situational awareness due to the integration of new technologies such as distributed renewable generation and electric vehicles. Recently, rapid growth in phasor measurement units (PMUs) has been observed in power systems. In the U.S., the number of PMUs was recorded to be around 1900 in 2017 with a nine-fold growth from 2009. Compared to the traditional power system monitoring devices, PMUs provide high-granularity (e.g., 30 or 60 samples per second) and synchronized measurements, including voltage and current phasor, frequency, and frequency variation, which enables capturing most dynamics of power systems. Hence, there has been much research on how to explore the PMU data to enhance system monitoring and control. One of the important applications is real-time event identification, which is directly related to event analysis [1]. The event identification models trained on PMU data not only provide supervisory monitoring but also maintain partial system awareness when supervisory control and data acquisition

This work is supported by the U.S. Department of Energy Office of Electricity under DEOE0000910 (*Corresponding author: Zhaoyu Wang*)

Y. Yuan, Z. Wang, and Y. Wang are with the Department of Electrical and Computer Engineering, Iowa State University, Ames, IA 50011 USA (e-mail: yuanyx@iastate.edu; wzy@iastate.edu).

(SCADA) is dysfunctional, as was the case during the 2003 North American large-scale blackout [2].

In recent years, a number of papers have explored data-driven methods for event detection and identification using PMU data. The previous work in this area can be roughly classified into two categories based on the number of PMUs used for model development: *Class I*: each PMU is treated independently and a single PMU data stream for each event is assigned as one data sample [3]–[6]. In [3], a signal processing-based methodology consisting of the swinging door trending algorithm and dynamic programming was proposed to detect power events. In [4], using real-world data in Korea, a wavelet-based model was developed by observing the difference between voltage and frequency signals. In [5], an empirical model decomposition was utilized to assess power system events using wide-area post-event records. In [6], principal component analysis (PCA) was used to detect abnormal system behavior and adopt system visualizations. *Class II*: Instead of using data from a single PMU, several papers perform event identification tasks using multiple PMU measurements, which integrate interactive relationships of different PMUs [7]–[11]. In these methods, the data of each event that includes multiple PMU data streams is assigned as one data sample for model development. In [7], a scheme was proposed for supervisory protection and situational awareness, which presented a new metric to identify PMU with the strongest signature and an extreme learning machine-based event classifier. In [8], a data-driven algorithm was proposed, which consists of an unequal-interval method for dimensionality reduction and a PCA-based search method for event detection. The basic idea is to measure similarities and local outlier factors between any two PMU data streams. In [9], a data-driven event identification method was proposed by characterizing an event utilizing a low-dimensional row subspace spanned by the dominant singular vectors of a high-dimensional spatial-temporal PMU data matrix. In [10], a minimum-volume ellipsoid method was proposed for event detection by selecting three PMU measurements. In [11], a correlation-based method was developed to concurrently monitor multiple PMU data streams for identifying system events.

While these methods have led to meaningful guidelines and invaluable insights, some questions remain open with respect to real-time PMU-based event identification. Basically, Class I models rely on a single PMU for model development. This means each PMU is treated independently and their interactions are ignored, which lowers the accuracy and reliability of identification results. Moreover, the results obtained by

using the data of a single PMU to identify power system events may be uncomprehensive and unreliable in practice. On the other hand, Class II methods are generally based on the simplified assumption that each PMU has the same interactive relationship with the rest of PMUs (using a fully-connected graph to represent interactive graphs). However, such an assumption may not be realistic due to the complexity of power systems. A natural way in tackling this problem is to directly learn the interactive graph from data [12]. To achieve this, there are several unsolved problems: 1) The correlation and causality relations can be utilized to describe the interaction relationships based on time and frequency domain coherency relation between dynamics observed at different PMUs. However, performing interaction learning and event identification separately would diminish accuracy. 2) The models that utilize multiple PMU data streams as the input may lead to a high computation complexity, which renders their practical implementation costly. 3) Some information (i.e., topology information) may be unavailable for researchers due to privacy protection. For example, we have been granted access to a dataset comprising tens of PMUs with a time span of two consecutive years without disclosure of the grid topology.

To tackle these problems, we propose a novel graphical event identification method that consists of data-driven interaction graph inference and graph neural network (GNN)-based event identification. Our model is trained in an end-to-end manner to maximize the event identification accuracy, which can *simultaneously optimize* the interaction graph inference and event identification task. In the interaction graph inference part, for each labeled event, the latent relationship representing the probability of the existence of an edge between a pair of PMUs is estimated using a deep graph representation learning algorithm [13]. Based on the latent graph relationship, a multi-layer graph structure is obtained via a deterministic graph sampling method. Since the sampled graph is discrete, the Gumbel-softmax reparametrization approach is applied to provide continuous relaxation and enable computation of gradients [14]. When the graph is obtained, data feature extraction is achieved by utilizing a dilated inception-based model. This model consists of multiple convolution layers with different dilated factors and max-pooling layers, which helps capture multi-scale features effectively with limited extra parameters [15]. Finally, the GNN is utilized to perform event identification by combining the data features and the constructed graph [16]. The main contributions of this paper can be summarized as follows:

- The proposed method learns the latent interaction graph jointly with the event identification model, thus improving the accuracy of the graph learning and ensure the seamless integration between the learned interactions and the event identification.
- Our method integrates spatial correlations of different PMUs without needing any prior knowledge, such as detailed system topology, which ensures the protection of sensitive information and the practicability of the proposed model.

TABLE I  
STATISTICAL SUMMARY OF THREE INTERCONNECTIONS.

	A	B	C
Start Time	07/21/2018	01/01/2016	01/01/2016
End Time	08/24/2019	12/31/2017	12/31/2017
Data Size	3 TB	5 TB	12 TB
Number of PMUs	215	43	188
Sample Rates [frames/s]	30	30/60	30
Total Number of Events	29	4854	1884
Number of Unlabeled Events	0	0	634
Resolution of Event Record	Daily	Minute	Minute

- Instead of generating a single statistical graph to represent pair-wise relationships among PMUs during different events, our approach produces different graphs for different power system events, which is consistent with the nature of power system events.
- The proposed model has been developed and tested based on a real-world PMU dataset. The large number of real event labels contained in this dataset provides a good foundation for developing an efficient and practical event identification model.

The rest of this paper is constructed as follows: Section II introduces the available PMU dataset and data pre-processing. In Section III, data-driven interactive relationship inference and graphical event identification are described. The numerical results are analyzed in Section IV. Section V presents research conclusions.

## II. DATA DESCRIPTION AND PRE-PROCESSING

The available data is obtained from 440 PMUs installed across three U.S. transmission interconnections that include Texas, Western, and Eastern Interconnection. The rates of sampling are 30 and 60 frames per second, and the measured variables include voltage and current phasor, system frequency, frequency variation rate, and PMU status flag. For convenience, let A, B, and C denote the three interconnections hereinafter. The dataset is stored as Parquet form and includes around two years of measurements, from 2016 to 2017. We have utilized Python and MATLAB to read and analyze the whole dataset, which is larger than 20 TB (around 670 billion data samples).

Apart from PMU measurements, real event labels are needed to provide the ground truths in developing a practical PMU-based event identifier. In this work, a total of 6,767 event labels, consisting of 6,133 known events and 634 unknown events (where the event type entry is empty or unspecified), are utilized to extract the event dataset. Each event label includes the interconnection number, start timestamp, end timestamp, event type, event cause as well as event description. The timestamps of these event labels are based on SCADA's outage alarm reception time in the control room. Also, the types of events have been verified using the corresponding protection relay records, ensuring the high confidence of the event labels. Due to sensitive information protection, this protection information is not available to us.

To prevent erroneous event detection due to data quality issues (i.e., bad data, dropouts, communication issues, and time

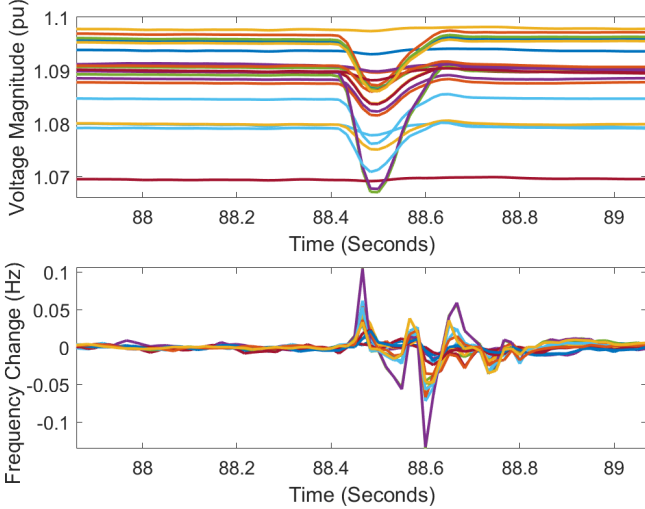


Fig. 1. Plots of multiple PMU data for a specific event.

errors), the PMU dataset is initially passed through data pre-processing. Heterogeneous data quality issues are classified based on the PMU status flags information. Following our data quality assessment, when a consecutive data quality issue occurs, the data is excluded from our study because it is hard to provide a high accuracy data imputation for these consecutive bad data points. The rest of the missing/bad data are filled and corrected through interpolation. In this work, a 2-second analysis-window is selected to ensure that our model can be implemented in real-time. It is clear that the 2-second window cannot cover certain events. However, we do not need all event information for identification model development. Basically, the analysis-window only needs to cover a small portion of the event data to provide sufficient event features for identifying event types. The 2-second window is determined based on the previous works and observations of real PMU data [2], [17]. Since the resolution of available event logs is in the order of minutes, thus, we have used a statistical method to reach a finer scale [18]. It should be noted that this statistical algorithm can be bypassed if the resolution of event logs is in the order of seconds. To simulate the real situation faced by the system operators, any manual changes to the event labels are avoided in this work. Note that even though the structure of the proposed model is *fine-tuned* on our dataset, the methodology is general and can be applied to any PMU datasets after some fine-tuning procedures. This is true for any data-driven solution.

### III. GRAPHICAL PMU-BASED EVENT IDENTIFICATION

In this section, we lay out our graphical event identification method. This method is motivated by insights from real PMU data. Fig. 1 shows the voltage magnitude values and frequency variations of all PMUs in interconnection B for a specific event. Based on this figure, it is clear that all PMUs in an area have captured the event. However, even though the nature of the variations in PMU data will be similar (i.e., event patterns and start timestamps are almost the same), the amount of variations will be different [2]. Further, as

is demonstrated in the figure, several PMUs show negligible event patterns, which should be excluded from the inputs to the event identification model. To achieve this, one simple solution is to select the PMU that shows the biggest impact based on context information or specific metrics [7]. However, context information may be unavailable *a priori* and metrics are hard to calculate in real-time. In this work, we propose a more natural solution that utilizes the data of all PMUs as the input of the model and automatically selects the suitable PMUs and the associated data by discovering interaction graphs. Moreover, PMU-based event identification via original data (i.e., voltage magnitude and frequency) is also a challenging task due to the non-stationary characteristics of real-world PMU data caused by sudden variations in system behavior during events [4]. In response to this problem, an efficient multi-scale feature extraction scheme is leveraged in this work. It should be noted that these two parts are trained simultaneously to ensure the optimality of the graph learning procedure.

In general, our model has an auto-encoder-based structure: an encoder that infers the interaction graph given multiple PMU data streams, and a decoder that automatically extracts data features and performs graphical event classification by combining the features and the constructed graph. The overall model is schematically described in Fig. 2. Our work follows the line of research that learns to infer relational graphs while learning the dynamics from observational data [13] [19]. Unlike previous methods that have focused on data prediction, the proposed method is capable of extracting the multi-scale event features and perform accurate event identification. Moreover, since interactions among different PMUs are impacted by the event location, our approach produces one graph structure for each event rather than one single statistics-based graph. Compared with the existing bilevel optimization-based graph learning approach [19], the graph structure in our model is parameterized by neural networks rather than being treated as a parameter, thus significantly reducing the computation burden during the training process. In addition, the online computation cost of the proposed learning-based method is much lower than the optimization-based method, thanks to the neural network implementation. In the following, we describe the proposed model in detail.

#### A. Interaction Graph Inference and Sampling

Let us first settle the notations. In this work, each PMU and the corresponding data (i.e., voltage magnitude value) can be considered as a *node* and *initial node feature*. Initial node features consist of  $\{\mathbb{V}, \mathbb{L}\}$ , where  $\mathbb{V} := \{v_1, \dots, v_h\}$  is the voltage magnitude set from PMUs,  $\mathbb{L} := \{l_1, \dots, l_h\}$  is the corresponding event label set from the event logs, and  $h$  is the total number of events. Specifically,  $v_i \in \mathbb{R}^{N \times T}$  is a set of voltage magnitude collected from  $N$  PMUs during event  $i$  within time windows with length  $T$ . Note that all PMU data for a specific event is considered as one data sample in this work.

The goal of the encoder is to compute the latent relationship  $\mathbb{E}_{i,j} := \{e_{i,j}^1, \dots, e_{i,j}^N\}$ , where  $e_{i,j}$  represents the probability of edge existence between PMUs  $i$  and  $j$ . To achieve this,

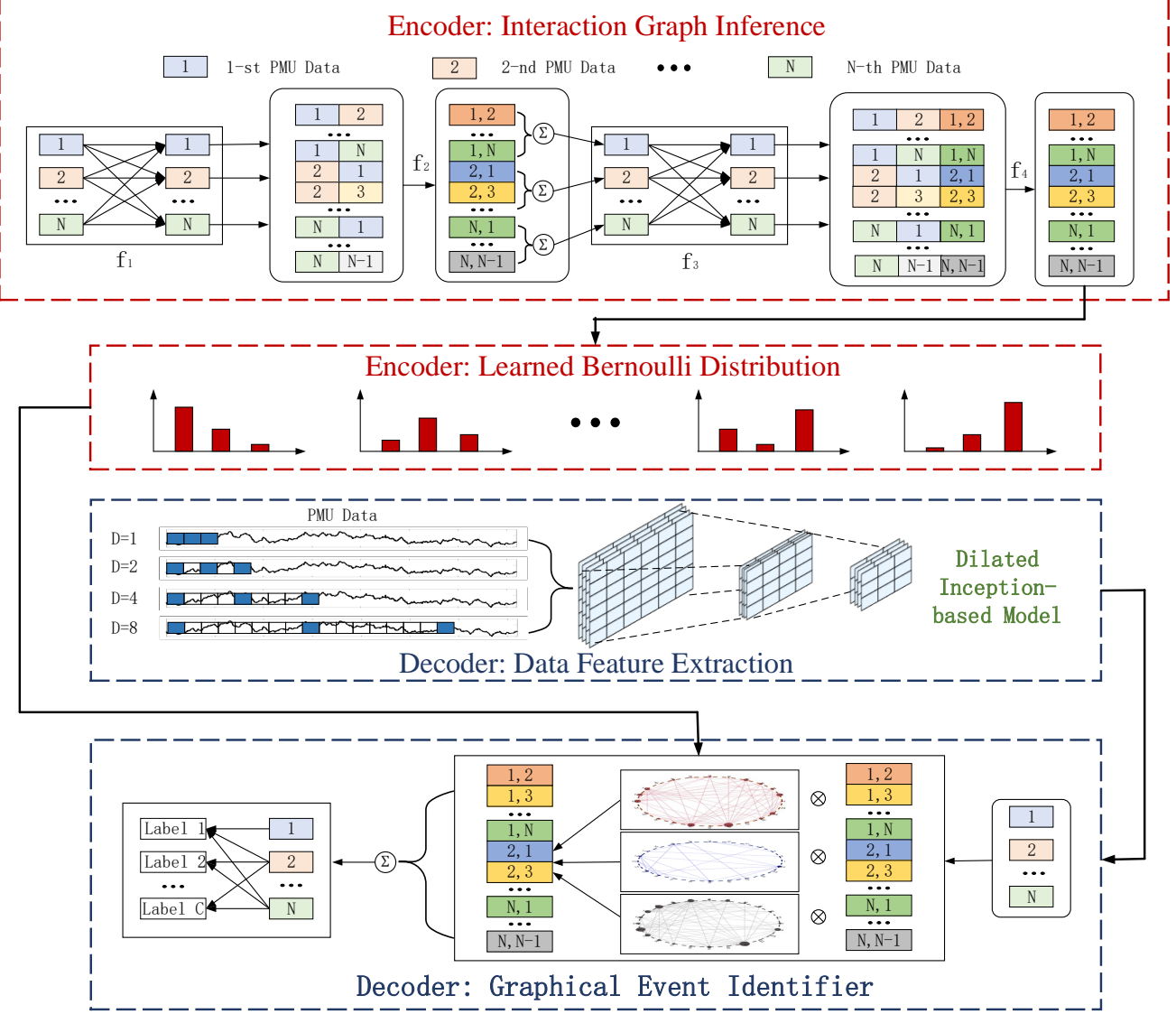


Fig. 2. Overall structure of the proposed method.

we utilize the recently-developed neural network technology to pass local information [20]:

$$e_{i,j}^k = f_e^k([e_i^k, e_j^k, x_{(i,j)}]) \quad (1)$$

$$e_i^{k+1} = f_n^k([\sum_{j \in N_i} e_{i,j}^k, x_i]) \quad (2)$$

where,  $e_i^k$  is the feature of node  $i$  in layer  $K$ ,  $e_{i,j}^k$  is the feature of the edge connecting nodes  $i$  and  $j$ ,  $N_i$  is the edge set that connects with node  $i$ ,  $x_i$  and  $x_{(i,j)}$  summarizes initial node and edge features, respectively, and  $[\cdot, \cdot]$  denotes the concatenation operation. The functions  $f_e$  and  $f_n$  are node and edge-based neural networks. Fig. 3 illustrates this operation. When a feature is transferred from a node to an edge (see Fig. 3 a),  $e_{1,2}^k$  is calculated based on the features of node 1 and 2,  $\{e_1^k, e_2^k\}$ . In other words, the node-to-edge operation represents concatenation of node features connected by an edge. Then, when a feature is transferred from edges to a

node (see Fig. 3 b),  $e_1^k$  is obtained by aggregation of edge features from edges that are connected to node 1. Since we do not assume any prior knowledge about underlying PMU-based interaction graph, this operation is used on the fully-connected graph (without self-loops). Based on Eq. 1 and 2, the encoder includes four steps to infer the  $\mathbb{E}_{i,j}$ :

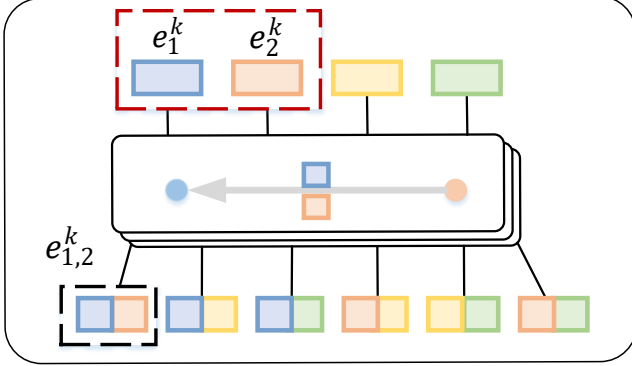
$$e_i^1 = f_1(v_i) \quad (3)$$

$$\text{Node} \rightarrow \text{Edge} : e_{i,j}^1 = f_e^1([e_i^1, e_j^1]) \quad (4)$$

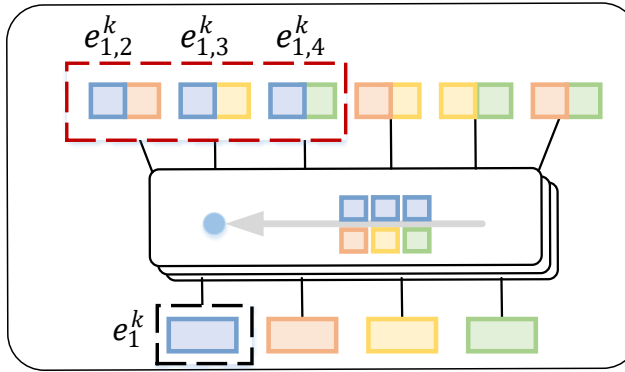
$$\text{Edge} \rightarrow \text{Node} : e_i^2 = f_n^1(\sum_{j \neq i} e_{(i,j)}^1) \quad (5)$$

$$\text{Node} \rightarrow \text{Edge} : e_{i,j}^2 = f_e^2([e_i^2, e_j^2]) \quad (6)$$

Following the previous research [13], two-layer fully-connected neuron networks (MLPs) are utilized for  $f_1$ ,  $f_e^1$ ,  $f_n^1$ , and  $f_e^2$  functions. It should be noted that the layer of the graph is determined by the number of output neurons in  $f_e^2$ ,



(a) Node to Edge



(b) Edge to Node

Fig. 3. Graph inference procedure.

which is set as 3 in this work. The exponential linear unit is used as the activation function in these networks. Compared to the commonly-used rectified linear unit, it has been proved that the exponential linear units can obtain higher classification accuracy [21]. Also, to avoid the internal covariate shift during training, a batch normalization layer is added after the activation layer [22]. Specifically, the normalization is achieved by subtracting the batch mean and dividing by the batch standard deviation.

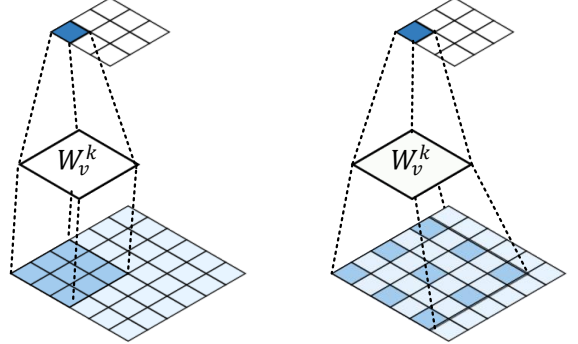
Using  $\mathbb{E}_{i,j}$ , the interaction graph is obtained via a graph sampling technique. Here, we apply a deterministic thresholding method as follows:

$$w_{i,j} = \begin{cases} 1 & \text{if } \text{sigmod}(e_{i,j}) > r \\ 0 & \text{otherwise} \end{cases} \quad (7)$$

where,  $r$  is a user-defined threshold. The deterministic thresholding method encourages sparsity if  $r$  gets closer to 1. Such a discrete graph, however, imposes a challenge on differentiability. In other words, the model parameters cannot be learned through backpropagation. To tackle this issue, we have utilized the Gumbel-Max trick that provides an efficient way to draw samples from a categorical distribution [14]. The detailed function is described as follows:

$$z = \text{one\_hot}(\arg \max_m [g_m + \log e_{i,j}^m]) \quad (8)$$

where,  $g_1, \dots, g_N$  are independent and identically distributed (i.i.d.) samples drawn from Gumbel distribution with 0 location



Standard convolution + max pooling 2-dilated convolution + max pooling

Fig. 4. Illustrate of the two dilated convolutional layers and max-pooling layers.

and 1 scale parameters<sup>1</sup>. Then, the softmax function is utilized as a differentiable approximation to  $\arg \max$ :

$$z_{i,j} = \frac{\exp((\log(e_{i,j}^m) + g_m)/\tau)}{\sum_{m=1}^N \exp((\log(e_{i,j}^m) + g_m)/\tau)} \quad (9)$$

where,  $\tau$  is a smooth coefficient and is assigned as 0.5 in this work. When  $\tau \rightarrow 0$ , this approximated distribution converges to one-hot samples from  $\mathbb{E}_{i,j}$ .

### B. Feature Extraction and Event Identification

The goal of the decoder is to construct a mapping relationship between the PMU data and the event types. The basic idea is to fit a boundary in the high-dimensional space to separate the data samples of different event types. To achieve superior identification performance in both accuracy and efficiency, it is imperative to devise a good feature extractor. In our previous work [18], a Markov-based feature extractor is utilized to capture the multi-scale data features. However, this feature extractor has an exponential computation burden in the dimension of the data samples, which is not appropriate in this work due to the extremely high-dimensional input. Hence, a new PMU-based feature extractor, dilated inception-based network, is proposed to capture multi-scale features effectively [23].

The proposed feature extractor follows the widely-used inception network developed by Google [24]. Unlike the original network that leverages parallel standard convolution layers with different kernel sizes, our network leverages parallel dilated convolution layers with different dilation rates, which can significantly reduce the complexity of the model. The main idea of dilated convolution is to insert zeros between two consecutive features in the convolutional kernels, which significantly increases the receptive field<sup>2</sup>. In general, the dilated convolution operation is defined as:

$$y[i] = \sum_l x[i + r \cdot l] w[l] \quad (10)$$

<sup>1</sup>Gumbel distribution with 0 location and 1 scale parameters can be sampled based on inverse transform method: draw  $u \sim$  standard uniform distribution and compute  $g = -\log(-\log(u))$ .

<sup>2</sup>In a deep learning context, the receptive field is the region in the input space that produces the feature.

where,  $r$  is a dilation factor. For a  $n \times n$  dilated kernel filter, the actual size of the receptive field is  $n_d \times n_d$ , where  $n_d = n + (n - 1) \cdot (r - 1)$ . This indicates higher  $r$  captures more slowly-varying features over larger temporal windows. When  $r$  equals 1, the standard discrete convolution is simply the 1-dilated convolution. A comparison between standard convolution and dilated convolution is described in Fig. 4. It is clear that a dilated  $3 \times 3$  convolutional kernel with  $r = 2$  has a similar receptive field with a standard  $5 \times 5$  convolutional kernel. To achieve multi-scale feature extraction, four dilated convolutions with various dilation rates are used in a parallel way. After each dilated convolution layer, a max-pooling layer is added to summary feature maps, thus further reducing the complexity of our model. As a result, a feature matrix is obtained:  $U_i = \{u_{i,1}, \dots, u_{i,T'}\}$ , where  $T'$  is the reduced data length.

When the PMU features are obtained, the GNN is utilized to perform the event identification task [16]. Compared to the previous machine learning-based methods that only use the data features as the input of the model, our event identifier combines the data features and the constructed graph. To achieve that, we use the node-to-node operation (see Eq. 1 to 2). First, the node-to-edge operation is performed to the extracted edge feature. Second, the obtained graph structure is combined with the edge feature using element-wise multiplication ( $\otimes$ ). Then the graph-based aggregation and edge-to-node operation are implemented, as shown in Fig. 2. Similar to the encoder, the node-based function is represented by a two-layer fully-connected network that includes exponential linear units as the activation function. The event classifier is achieved by adding a two-layer fully-connected network in the end. It is assigned a weight to each neuron that prioritizes the most appropriate event type. In this fully-connected layer, the softmax activation function is applied to normalize the output to a probability distribution over estimated event types, which is commonly used as the last activation function of a classification model.

Considering that the hyperparameters of all machine learning model (i.e., the number of layers and neurons, the dilation rate, the deterministic threshold) will affect the performance, the model has to be well-designed. The rationale behind the model designing is to make a trade-off between model complexity and identification accuracy. Hence, we utilize the random search method to find the appropriate hyperparameter sets in this work [25]. Basically, the value of the hyperparameter is chosen by "trial and error". It is hard to say that the selected hyperparameters are optimal, but these hyperparameters can provide good accuracy in the available real-world dataset with the limited model complexity. Specific values of hyperparameters are listed in the numerical section. For model training, the adaptive moment estimation (Adam) algorithm is used to update the learning parameters (i.e., weights and bias) of the proposed model [26]. Adam is an adaptive learning rate optimization for training deep neural networks. Based on adaptive estimates of lower-order moments, Adam can compute individual adaptive learning rates for each parameter, which significantly increases the training speed [26].

TABLE II  
THE STRUCTURE OF THE GRAPHICAL EVENT IDENTIFICATION MODEL.

Layout	Type	Output Shape
1/1	2-layer MLP	(16,24,256)
1/2	Batch normalization	(16,24,256)
1/3	Node-edge operation	(16,552,256)
2/1	2-layer MLP	(16,552,256)
2/2	Batch normalization	(16,552,256)
2/3	Edge-node operation	(16,24,256)
3/1	2-layer MLP	(16,24,256)
3/2	Batch normalization	(16,24,256)
3/3	Node-edge operation	(16,552,256)
4/1	2-layer MLP	(16,552,256)
4/2	Batch normalization	(16,552,256)
4/3	Fully-connected layer	(16,552,3)
5/1	Dilated-inception model (4 parallel dconv1d)	(384,32,30)
5/2	Dilated-inception model (4 parallel dconv1d)	(384,32,7)
5/3	Dilated-inception model (4 parallel dconv1d)	(384,32,1)
6/1	Fully-connected layer	(16, 1, 552, 256)
6/2	Activation layer	(16, 1, 552, 256)
6/3	Fully-connected layer	(16, 1, 552, 256)
6/4	Activation layer	(16, 1, 552, 256)
7/1	Fully-connected layer	(16, 256)
7/2	Activation layer	(16, 256)
7/3	Fully-connected layer	(16, 5)

### C. Overfitting Mitigation Strategy

The superior performance of deep learning models relies heavily on the availability of massive training data samples. Unlike our previous work that treats each PMU independently and enjoys a high level of data redundancy<sup>3</sup>, the proposed graphical model is trained with the limited event-based data samples. Therefore, it is imperative to deal with the overfitting problem. To facilitate a better understanding, we provide a simple explanation about the overfitting problem. Overfitting refers to a learning model that can only model the training data well. If a model suffers from an overfitting problem, the accuracy of the model for the unseen data is questionable. Hence, three strategies are utilized to eliminate the overfitting problem in this work.

**Dropout:** Dropout is a commonly-used regularization method to prevent a model from overfitting [27]. The basic idea of dropout is to randomly set the outgoing edges of hidden units to 0 at each iteration of the training procedure. In this work, based on the calibration results, the dropout ratio that specifies the probability at which outputs of the layer are temporarily dropping out is set as 0.3.

**Constraining model complexity:** As is demonstrated in Fig. 2, the proposed model possesses a relatively high model complexity compared to the conventional classification model due to the graph learning and multi-scale feature extractor. One natural way to reduce the risk of overfitting is to constrain model complexity [28]. To achieve this, the number of adaptive parameters (i.e., the number of hidden neurons in  $f_1$ ,  $f_e^1$ ,  $f_n^1$ , and  $f_e^2$  functions) in the network is reduced.

<sup>3</sup>In our previous PMU-based event identification model, we have utilized the data of a single PMU to construct a training dataset, which is more than 200,000 data samples.

TABLE III  
COMPARISON OF IDENTIFICATION ACCURACY FOR THREE METHODS.

Method	Testing accuracy
Proposed method	78%
CNN-based method [18]	60%
Support vector machine (SVM) [2]	63%

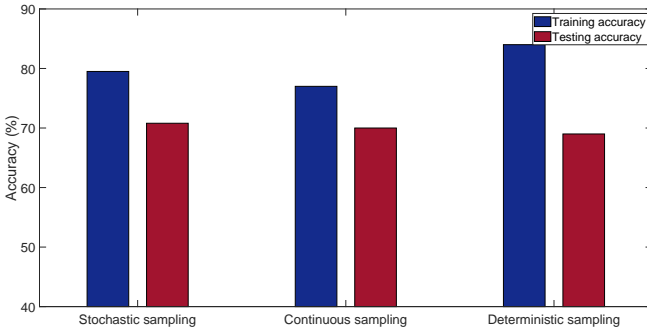


Fig. 5. Comparison of three different graph sampling methods.

**Data augmentation:** Theoretically, one of the best options for alleviating overfitting is to get more training data. It is well-known that collecting enough power event data is hard and time-consuming, yet we still could easily increase the size of the training dataset by leveraging data augmentation technology [29]. Here, we utilize a horizontally flipping method to obtain additional data samples. To eliminate the impact of the event location, in the data augmentation, we do the same procedure for all PMU signals in a given event. Moreover, the Gaussian noise with 0 mean and 0.04 variance is added to these additional data samples.

#### IV. NUMERICAL RESULTS

To evaluate the performance of the proposed graphical model, we test it on the real PMU datasets and the related event logs of the interconnection B. In this work, the whole dataset includes around 9600 data samples that consist of line outage, transformer outage (XFMR), frequency event, and normal condition. After data cleaning, the event dataset is randomly divided into three separate subsets for training (70% of the total data), validation (15% of the total data), and testing (15% of the total data). The case study is conducted on a standard PC with an Intel(R) Xeon(R) CPU running at 4.10GHZ and with 64.0GB of RAM and an Nvidia Geforce GTX 1080ti 11.0GB GPU. To determine whether the proposed method can provide real-time supervisory monitoring, it is necessary to calculate the testing time. Based on our standard PC, the average testing time for the proposed method is around 0.0156s that is short enough for real-time event identification, in accordance with the IEEE C37.118.2-2011 standard. The training time for the proposed method is around 10 hours. Considering that the training procedure of the proposed model is an offline process, the high computational burden of the training procedure does not impact the real-time performance of our event identification model.

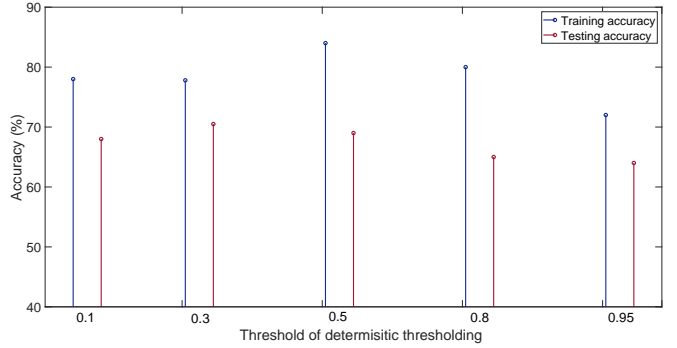


Fig. 6. Sensitivity of event identification accuracy to the graph sparsity.

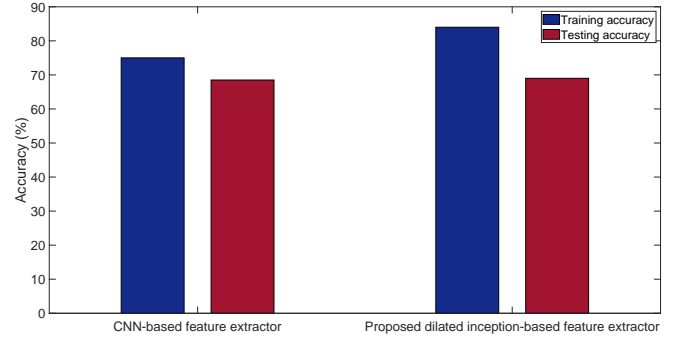


Fig. 7. Comparison of CNN-based feature extractor and proposed dilated inception-based feature extractor.

To help the reader understand each step of the proposed model, the detailed structure of the proposed PMU-based event identifier is presented in Table II. In the table, we provide the type and output shape for each layout. As can be seen, our model mainly includes seven parts to achieve interaction graph inference, data feature extraction, and graphical event identifier. Based on this model structure, the event classification performance of the proposed model is tested on the testing dataset. The accuracy index is applied to measure the performance, which is determined as follows [30]:

$$Accuracy = \frac{(TP + TN)}{(TP + FP + FN + TN)} \quad (11)$$

where, TP is the true positive, TN is the true negative, FP is the false positive, and FN is the false negative. Table III summarizes the accuracy that utilizes the deterministic thresholding method for graph sampling and data augmentation strategy for reducing overfitting and existing two methods, CNN-based method and SVM. To ensure a fair comparison between the three methods, the accuracies of the three methods are evaluated based on the same system-level criteria. Based on this table, it is clear that the proposed method has better performance (78%) than the other methods ({60%, 63%}) in this case, indicating that data-driven inference of interaction graphs can improve the accuracy of the event identification.

Furthermore, we show the accuracy of our model for various graph sampling methods and feature extractors. Note that the following results are obtained by using the same overfitting strategy (dropout). First, in Fig. 5, the perfor-

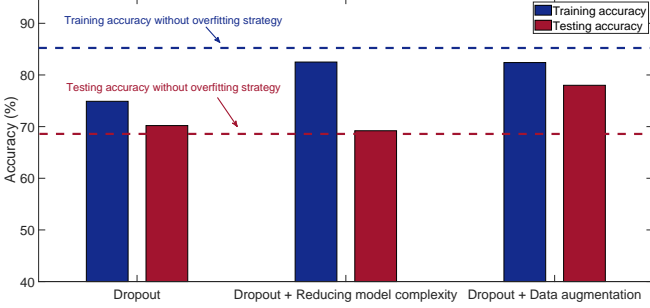
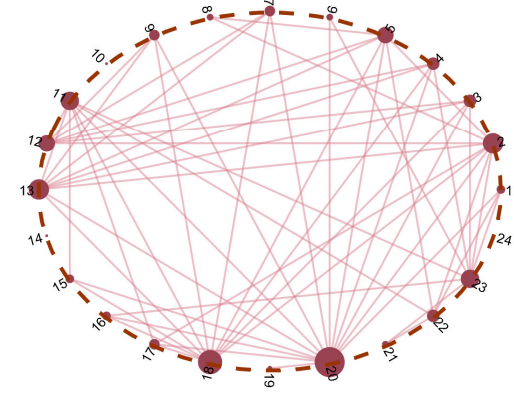


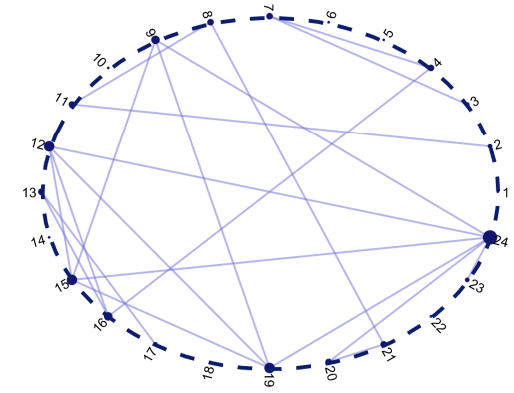
Fig. 8. Comparison of three overfitting strategies.

mance of three different graph sampling methods is compared, which includes stochastic sampling, continuous sampling, and deterministic thresholding. As is described in the figure, the training accuracy values for the three methods are  $\{77\%, 79.5\%, 84\%\}$ , respectively. And the testing accuracy values are  $\{70\%, 70.8\%, 69\%\}$ . Based on this dataset, the deterministic thresholding method shows a slightly better performance than two other sampling methods. Moreover, Fig. 6 is plotted to represent the sensitivity of the identification accuracy to the graph sparsity (the threshold of deterministic thresholding method). As is depicted in the figure, the performance of the proposed model can reach better accuracy with a moderate threshold value (around 0.5). Extremely high or low threshold values are inappropriate.

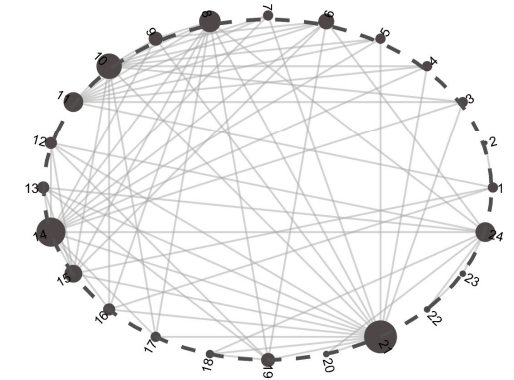
Then, two different feature extractors, namely the proposed dilated inception-based feature extractor and traditional CNN (including 3 convolutional and 2 max-pooling layers) are compared, as shown in Fig. 7. In this figure, the training and testing accuracy of the proposed dilated inception-based feature extractor,  $\{84\%, 69\%\}$ , are higher than the values of the traditional CNN structure,  $\{75\%, 68.5\%\}$ , which proves the enhancement of multi-scale feature extractor. However, based on Fig. 5, 6, and 7, it is observed that the difference between the training and testing accuracy is not trivial. This indicates that the dropout strategy falls short of dealing with the overfitting problem in this case. Hence, we have combined two other strategies: constraining model complexity and data augmentation. The corresponding accuracy values are presented in Fig. 8. As seen in this figure, the training accuracy decreases from around 84% to around 80%. However, the testing accuracy increases significantly compared to the previous cases. Specifically, in this case, the combination of dropout and data augmentation has the best performance in reducing the overfitting risk: the training and testing accuracy are  $\{82.4\%, 78\%\}$ . It is clear that the testing accuracy of the model will eventually achieve a similar level with the training accuracy if we can add more data samples. We are not surprised that the proposed method cannot achieve an accuracy of more than 90%. As mentioned in the previous works [2], [8], real-world datasets suffer from many uncertainties and imperfections, leading to degraded model performance. Furthermore, as described in Table.III, based on our numerical comparisons with two commonly-used classification algorithms: SVM and CNN, our method has the



(a) Representative graph structures for the first graph layer.



(b) Representative graph structures for the second graph layer.



(c) Representative graph structures for the third graph layer.

Fig. 9. Representative graph structures for all data. Each graph (red, green, and blue) corresponds to each graph layer. The size of a vertex is proportional to its in-degree.

lowest misclassification ratio.

Fig. 9 shows the representative graph structures that had the best performance under various cases (i.e., deterministic thresholding,  $r = 0.5$ , data augmentation, graph layer equals 3). Since the graph is different for each data, we aggregate all graphs and then select the most frequently appearing (top 10%) edges as the representation graph structures. Based on these figures, it is obvious that three graph layers are different and convey different interactive information. Compared to the first and the third graph layers, the second graph layer (Fig. 9

(b)) shows relatively sparse connections. Considering that no ground truth of the interactive relationships is available, it is hard to judge the correctness of the extracted graphs. Hence, to evaluate the performance of our data-driven interaction inference, we perform the Monte Carlo simulation and measure the dissimilarity of learned graphs over repeated simulations [31]. The rationale behind this is that a low level of dissimilarity among the learned graphs means that they are reliable and valuable. Here, we utilize a metric, D-measure, to quantify graph dissimilarities, which is calculated as follows [31]:

$$J(P_1, \dots, P_N) = \frac{1}{N} \sum_{i,j} p_i(j) \log \left( \frac{p_i(j)}{\frac{1}{N} \sum_{i=1}^N p_i(j)} \right) \quad (12)$$

$$\Phi(G) = \frac{J(P_1, \dots, P_N)}{\log(\eta + 1)} \quad (13)$$

$$\begin{aligned} D(G_1, G_2) = & 0.45 \cdot \sqrt{\frac{J(\mu_{G_1}, \mu_{G_2})}{\log 2}} + 0.45 \cdot |\sqrt{\Phi(G_1)} \\ & - \sqrt{\Phi(G_2)}| + 0.05 \cdot \left( \sqrt{\frac{J(\alpha_{G_1}, \alpha_{G_2})}{\log 2}} \right. \\ & \left. + \sqrt{\frac{J(\alpha_{G_1^c}, \alpha_{G_2^c})}{\log 2}} \right) \end{aligned} \quad (14)$$

where,  $P_i$  is the distance distribution of node  $i$  in graph  $G$ ,  $\eta$  is the graph's diameter,  $\alpha_{G_1}$  and  $\alpha_{G_2}$  are the  $\alpha$ -centrality values of  $G_1$  and its complements. Mathematically,  $D_{G_1, G_2} = 0$  only if  $G_1$  and  $G_2$  have the same graph distance distribution, the same graph node dispersion, and the same  $\alpha$ -centrality vector. In general, low D-measure indicates that the dissimilarity of the two learned graphs is small. In this work, based on 100 simulations, the average D-measure is relatively low, which is around 0.3. This result shows that the data-driven interaction inference works reliably, and the learned graphs are meaningful.

## V. CONCLUSION

In this paper, we have presented a novel graphical data-driven method for real-time event identification using PMU data. Compared to previous works in the literature, the proposed approach provides a basis to take full advantage of all PMUs in systems for event identification and does not require any prior knowledge of interactive relationships (i.e., detailed topology information). Furthermore, our model simultaneously optimizes the data-driven inference of graph and event identification task, thus ensuring the optimality of the graph inference procedure. Different strategies are applied to reduce the model complexity. Based on a large-scale PMU dataset and the related event logs, the proposed event identification method provides a higher accuracy compared to the existing methods. Our future work will extend the proposed graphical method for event localization once we acquire the system topology and historical event locations.

## ACKNOWLEDGMENT AND DISCLAIMER

Acknowledgment: "This material is based upon work supported by the Department of Energy under Award Number DE-OE0000910."

Disclaimer: "This report was prepared as an account of work sponsored by an agency of the United States Government. Neither the United States Government nor any agency thereof, nor any of their employees, makes any warranty, express or implied, or assumes any legal liability or responsibility for the accuracy, completeness, or usefulness of any information, apparatus, product, or process disclosed, or represents that its use would not infringe privately owned rights. Reference herein to any specific commercial product, process, or service by trade name, trademark, manufacturer, or otherwise does not necessarily constitute or imply its endorsement, recommendation, or favoring by the United States Government or any agency thereof. The views and opinions of authors expressed herein do not necessarily state or reflect those of the United States Government or any agency thereof."

## REFERENCES

- [1] J. D. L. Ree, V. Centeno, J. S. Thorp, and A. G. Phadke, "Synchronized phasor measurement applications in power systems," *IEEE Trans. Smart Grid*, vol. 1, no. 1, pp. 20–27, 2010.
- [2] S. Brahma, R. Kavasseri, H. Cao, N. R. Chaudhuri, T. Alexopoulos, and Y. Cui, "Real-time identification of dynamic events in power systems using pmu data, and potential applications—models, promises, and challenges," *IEEE Trans. Power Deli.*, vol. 32, no. 1, pp. 294–301, Feb. 2017.
- [3] M. Cui, J. Wang, J. Tan, A. R. Florita, and Y. Zhang, "A novel event detection method using pmu data with high precision," *IEEE Trans. Power Systems*, vol. 34, no. 1, pp. 454–466, 2019.
- [4] D. Kim, T. Y. Chun, S. Yoon, G. Lee, and Y. Shin, "Wavelet-based event detection method using pmu data," *IEEE Trans. on Smart Grid*, vol. 8, no. 3, pp. 1154–1162, 2017.
- [5] M. K. Jena, B. K. Panigrahi, and S. R. Samantaray, "A new approach to power system disturbance assessment using wide-area postdisturbance records," *IEEE Trans. on Industrial Informatics*, vol. 14, no. 3, pp. 1253–1261, 2018.
- [6] T. Xu and T. Overbye, "Real-time event detection and feature extraction using pmu measurement data," in *Proc. IEEE Int. Conf. Smart Grid Commun.*, pp. 265–270, 2015.
- [7] M. Biswal, S. M. Brahma, and H. Cao, "Supervisory protection and automated event diagnosis using pmu data," *IEEE Trans. Power Deli.*, vol. 31, no. 4, pp. 1855–1863, 2016.
- [8] S. Liu, Y. Zhao, Z. Lin, Y. Liu, Y. Ding, L. Yang, and S. Yi, "Data-driven event detection of power systems based on unequal-interval reduction of pmu data and local outlier factor," *IEEE Trans. Smart Grid*, vol. 11, no. 2, pp. 1630–1643, 2020.
- [9] W. Li, M. Wang, and J. H. Chow, "Real-time event identification through low-dimensional subspace characterization of high-dimensional synchrophasor data," *IEEE Trans. Power Systems*, vol. 33, no. 5, pp. 4937–4947, 2018.
- [10] Y. V. Makarov, C. H. Miller, T. B. Nguyen, and Jian Ma, "Monitoring of power system dynamic behavior using characteristic ellipsoid method," *Proceedings of the 41st Annual Hawaii International Conference on System Sciences (HICSS 2008)*, pp. 186–186, 2008.
- [11] R. Meier, B. McCamish, E. Cotilla-Sanchez, J. Landford, R. B. Bass, and D. Chiu, "Event detection using correlation within arrays of streaming pmu data," pp. 1–5, 2018.
- [12] S. Abdulla, M. Diykh, R. L. Laft, K. Saleh, and R. C. Deo, "Sleep eeg signal analysis based on correlation graph similarity coupled with an ensemble extreme machine learning algorithm," *Expert Systems with Applications*, vol. 138, pp. 186–186, 2019.
- [13] T. Kipf, E. Fetaya, K.-C. Wang, M. Welling, and R. Zemel, "Neural relational inference for interacting systems," *arXiv preprint arXiv:1802.04687*, 2018.

- [14] E. Jang, S. Gu, and B. Poole, “Categorical reparameterization with gumbel-softmax,” *In Proceedings of the 5th International Conference on Learning Representations*, pp. 1–12, 2017.
- [15] W. Shi, F. Jiang, and D. Zhao, “Single image super-resolution with dilated convolution based multi-scale information learning inception module.” *In Proceedings of the IEEE International Conference on Image Processing*, pp. 977–981, 2017.
- [16] S. Jang, S. Moon, and J. Lee, “Brain signal classification via learning connectivity structure,” *arXiv preprint arXiv:1905.11678*, 2019.
- [17] W. Gao and J. Ning, “Wavelet-based disturbance analysis for power system wide-area monitoring,” *IEEE Transactions on Smart Grid*, vol. 2, no. 1, pp. 121–130, 2011.
- [18] Y. Yuan, Y. Guo, K. Dehghanpour, Z. Wang, and Y. Wang, “Learning-based real-time event identification using rich real pmu data,” *arXiv preprint arXiv:2006.10121*, 2020.
- [19] L. Franceschi, M. Niepert, M. Pontil, and X. He., “Learning discrete structures for graph neural networks,” *ICML*, pp. 1–1, 2019.
- [20] G. Justin, S. S. Schoenholz, P. F. Riley, O. Vinyals, and G. E. Dahl, “Neural message passing for quantum chemistry,” *ICML*, pp. 1–1, 2017.
- [21] D.-A. Clevert, T. Unterthiner, and S. Hochreiter, “Fast and accurate deep network learning by exponential linear units (elus),” *arXiv preprint arXiv:1511.07289*, 2016.
- [22] S. Ioffe and C. Szegedy, “Batch normalization: Accelerating deep network training by reducing internal covariate shift,” *arXiv preprint arXiv:1502.03167*, 2015.
- [23] S. Yang, G. Lin, Q. Jiang, and W. Lin, “A dilated inception network for visual saliency prediction,” *arXiv preprint arXiv:1904.03571*, 2019.
- [24] C. Szegedy, W. Liu, Y. Jia, P. Sermanet, S. Reed, D. Anguelov, D. Erhan, V. Vanhoucke, and A. Rabinovich, “Going deeper with convolutions,” *in Proceedings of the IEEE conference on computer vision and pattern recognition*, pp. 1–9, 2015.
- [25] J. Bergstra and Y. Bengio, “Random search for hyper-parameter optimization,” *Journal of Machine Learning Research*, vol. 13, pp. 281–305, Feb. 2012.
- [26] Kingma, D. P., and J. Ba, “Adam: A method for stochastic optimization,” *arXiv preprint arXiv:1412.6980*, 2014.
- [27] S. Nitish, G. Hinton, A. Krizhevsky, I. Sutskever, and R. Salakhutdinov, “Dropout: a simple way to prevent neural networks from overfitting,” *The journal of machine learning research*, vol. 15, no. 1, pp. 1929–1958, 2014.
- [28] I. Goodfellow, Y. Bengio, and A. Courville, *Deep Learning*. MIT Press, 2016, <http://www.deeplearningbook.org>.
- [29] Q. Wen, L. Sun, X. Song, J. Gao, X. Wang, and H. Xu, “Time series data augmentation for deep learning: A survey,” *arXiv preprint arXiv:2002.12478*, 2020.
- [30] T. Fawcett, “An introduction to roc analysis,” *Pattern Recognition Letters*, vol. 27, no. 8, pp. 861–874, Jun 2006.
- [31] T. A. Schieber, L. Carpi, A. Diaz-Guilera, P. M. Pardalos, C. Masoller, and M. G. Ravetti, “Quantification of network structural dissimilarities,” *Nature communications*, vol. 8, no. 1, pp. 1–10, 2017.